Combustion regime identification from machine learning trained by Raman/Rayleigh line measurements

Kaidi Wan, Sandra Hartl, Luc Vervisch, Pascale Domingo, Robert Barlow, Christian Hasse

Combustion regime identification from machine learning trained by Raman/Rayleigh line measurements

Kaidi Wan[a,*], Sandra Hartl[b], Luc Vervisch[a], Pascale Domingo[a],
Robert S. Barlow[c], Christian Hasse[b]

[a]*CORIA – CNRS, Normandie Université, INSA Rouen Normandie, 76801 Saint-Etienne-du-Rouvray, France*
[b]*Institute for Simulation of Reactive Thermo-Fluid-Systems, TU Darmstadt, Darmstadt, Germany*
[c]*Combustion Research Facility, Sandia National Laboratories, Livermore, CA, USA*

Abstract

A combustion regime identification based on convolutional neural networks (CNNs) is developed using the recently proposed gradient-free regime identification (GFRI) approach applied to two turbulent CH_4/air jet flames featuring multi-regime characteristics. The training and the subsequent application of the CNN rely on the processing of one-dimensional Raman/Rayleigh line measurements of species mass fractions and temperature (CNN input). The combustion regime index is then readily predicted at every point along the measured line (CNN output). For training the neural network, the combustion regime index is first determined using the GFRI method (Hartl et al., 2018) based on the chemical explosive mode analysis (CEMA). Six classes of combustion regimes, including premixed (P), dominantly premixed (DP), multi-regime (MR), dominantly non-premixed (DNP), non-premixed (NP), and lean back-supported (LBS), are well detected by the trained CNN, with a pixel-wise accuracy of more than 85% for burner operating conditions unseen during training (different free-stream equivalence ratios). The quasi instantaneous neural network response provides a perspective towards real-time global combustion regime identification for pollutants emission control. From the results, it is also concluded that introducing physical insight, by combining advanced experimental (Raman/Rayleigh line measurements) and numerical analysis (GFRI), allows for reducing the amount of data needed to train neural networks.

Keywords: Convolutional neural network, Combustion regime, Raman/Rayleigh, Flame regime marker, Gradient-free regime identification

1. Introduction

Complex multi-regime combustion scenarios, including premixed, partially premixed and non-premixed flames, are commonly reported in combustion systems due to partial premixing of the reactants before they enter the reaction zones, or because of strong finite rate chemistry effects, or even local quenching. The so-called Takeno's flame index [1] is the most popular identifier of local combustion regimes. This flame index exploits information on the degree of alignment between fuel and oxidiser gradients, to determine the nature of the local combustion regime ranging between the two canonical ones, premixed flame (fuel and oxidizer gradients pointing in the same direction) and diffusion flame (gradients in opposite directions). This indicator and its slightly modified versions have been popularised by the analysis of the topological properties of reaction zones in direct numerical simulation (DNS) [2–4] and large-eddy simulation (LES) [5–7]. Because they require the knowledge of three-dimensional gradients of multiple scalars, these combustion regimes identifiers, and others based on molecular diffusive fluxes estimations [6, 8, 9], have seldom been extended to experimental measurements [10].

Recently, Hartl et al. [11, 12] proposed a novel combustion regime characterization solely relying on spatial one-dimensional Raman/Rayleigh line measurements of major species concentrations and temperature. In this approach, to complement the knowledge of the Raman/Rayleigh accessible major species and temperature, the full thermochemical state is first approximated by simulating a homogeneous constant-pressure and constant-temperature reactor. After the radicals and minor species have built up, the heat release rate (HRR) is calculated and the chemical explosive mode analysis (CEMA) is performed [13]. These two key flame markers are then combined with the mixture fraction (or local equivalence ratio), to identify different combustion regimes, thanks to a gradient-free regime identification (GFRI) strategy [11, 12]. It was evaluated using DNS of stratified flames [14] and applied to a lifted flame experiment [15] and to the Darmstadt multi-regime burner configuration [12]. In the latter work, GFRI was extended by an automated procedure to characterize local flame structures based on the relative HRR from premixed and non-premixed reaction zones in close proximity.

*Corresponding author
Email address: kaidi.wan@coria.fr (Kaidi Wan)

This gradient-free combustion regime identification has been shown to be robust and accurate. Nonetheless, a quite large amount of CPU time is required to process the measurements and predict the corresponding combustion regime. Indeed, the pointwise approximation of the full thermochemical state, is obtained by numerically converging solutions of homogeneous reactors with a detailed chemical scheme. In addition, the CEMA analysis requires computing the eigenvalues of the chemical Jacobian matrix to get the chemical explosive mode for every point of the one-dimensional line. In the end to fully analyse turbulent jet flame measurements, the overall procedure usually take hours on a regular workstation

Machine learning technologies are based on learning from a database to then make predictions. These methods belongs to a rapidly growing field [16–18]. One of the machine learning technologies based on convolutional neural networks (CNNs), which was originally developed for analyzing visual representations [19, 20], has been recently introduced in combustion modeling [21–23] and flame control [24]. In the present study, the gradient-free identification regime is combined with CNN, to provide an ultra-fast and reliable combustion regime determination based on thermochemical properties.

The experimental database is detailed in the subsequent section along with the proposed machine learning procedure trained from the GFRI automated classification. Then, the developed approach is tested over two different databases to examine its capability of combustion regime identification.

2. Methodology

2.1. 1D Raman/Rayleigh measurement database

One-dimensional Raman/Rayleigh/CO-LIF line imaging has been collected on the multi-regime burner (MRB) configuration with the experimental apparatus detailed in [12]. The burner consists of three co-flowing inlet streams, a central jet and two slots (Table 1). The ensemble is protected from the environment by an additional air coflow at 1 m/s. To facilitate laser measurements in the vicinity of the burner, the three inlet streams are inclined by 26° from each other. The central jet tube, with an inner and outer diameters of 3.0 mm and 3.3 mm, respectively, is surrounded

by the first annular slot of 7.0 mm diameter, followed by a second annular slot between 40 mm and 60 mm from the burner centerline. The outer diameter of the burner is 80 mm. Varying the equivalence ratios of the jets, numerous combustion regimes have already been reported [12].

Two cases summarized in Table 1 are considered thereafter. Flame MRB18b lies slightly outside the rich flammability limit, while MRB26b includes a large region of mixtures beyond the flammability limit, to promote non-premixed and multi-regime combustion scenarios.

Table 1: Multi-regime burner operating conditions [12]. u_b ($\mathrm{m \cdot s^{-1}}$) is the bulk velocity and ϕ the equivalence ratio.

Case	Central jet		Slot 1		Slot 2	
	u_b	ϕ	u_b	ϕ	u_b	ϕ
MRB18b	105	1.8	15	0	20	0.8
MRB26b	105	2.6	15	0	20	0.8

Single-shot distributions along 6 mm sample lines of species mass fractions, i.e., H_2, O_2, CO, CO_2, CH_4, H_2O, and N_2, and temperature are available with a data spacing of 20 μm for five downstream locations (h = 15, 22.5, 30, 60 and 90 mm) [12]. They have been obtained using spontaneous Raman scattering, Rayleigh scattering, and two-photon CO-LIF diagnostics, leading to more than 1000 samples for most measurement locations. These radial profiles were collected by traversing the burner in the direction of the laser axis.

The combustion regimes are first determined at every point of the sampled instantaneous lines via GFRI [11, 12]. In total six classes are considered: premixed (P), dominantly premixed (DP), multi-regime (MR), dominantly non-premixed (DNP), non-premixed (NP), and lean back-supported (LBS). These are obtained first defining regions of interest from the zero crossing of the chemical mode, then three reference values of the heat release rate within these regions are collected to build a normalized parameter η, used to delineate between the combustion regimes, see [12] for all the details on previously published GFRI method.

2.2. CNN regime identification approach

While traditional machine learning methods could address this problem point by point, CNN offers the possibility of analyzing the full profile in a single inference. In this so-called "image segmentation" approach, the input line is seen as a whole while the output classifies each pixel, thus preserving the locality of the information.

The CNN input is composed of the one-dimensional profiles, T, of temperature, and Y_i, of species mass fractions, H_2, O_2, CO, CO_2, CH_4, H_2O and N_2. The output is the one-dimensional distribution of combustion regime index ξ. The raw one-dimensional profiles have a non-uniform length ranging between 126 and 247 pixels. Various procedures have been tested to secure a uniform CNN input. Better results are obtained by filling the raw profiles with a fixed dummy value, to reach a uniform length of $256 = 2^8$ pixels. The dummy value used for the CNN input is zero, i.e., for species mass fractions and temperature, while it is 7 for the corresponding target combustion regime index. The combustion index ξ used here is an integer in the range [0, 7], corresponding to the six regimes, an additional not burning (NB) state and the dummy value, as summarized in Table 2. The samples without combustion over the entire line are not considered. The resulting numbers of sample lines used for each location of the two flames are summarized in Table 3.

The raw database contains 0.0001% of outlier values, which were dropped out. Then, the CNN operates with normalized quantities, thereby the seven species mass fractions and the temperature are normalized by their respective maximum values over the whole database. These maximum values are CO_2/0.205, O_2/0.233, CO/0.329, N_2/0.767, CH_4/0.074, H_2O/0.235, H_2/0.005, T (K)/2293.3.

In recent years, several architectures have been introduced for the image segmentation tasks, as fully convolutional network (FCN) [25], SegNet [26], U-Net [27] and fully convolutional DenseNet [28]. In the present study, a U-net inspired architecture is adopted because it provides good performance with a relatively simple network structure.

Originally the U-net is optimized for dealing with two-dimensional images, it is here adapted to one-dimensional information. As shown in Fig. 1, the CNN contains a downsampling (left side) and an upsampling path (right side). One downsampling step consists of two padded one-dimensional convolutions with a kernel of 3 (the dimension of the filter is the number of channels of the incoming layer $\times$ 3, e.g., at the first downsamping step following the input layer the dimension of the filter for the first convolution is 8×3, while that for the second convolution becomes 64×3), each followed by a rectified linear unit (ReLU) and a maxpooling operation with stride 2. The number of feature channels are doubled at each downsampling step. In practice, the number of

Table 2: Values of the combustion regime index ξ and corresponding regime.

ξ	Combustion regime	
0	Not burning	NB
1	Premixed	P
2	Dominantly premixed	DP
3	Multi-regime	MR
4	Dominantly non-premixed	DNP
5	Non-premixed	NP
6	Lean back-supported	LBS
7	Dummy value	

Table 3: Number of line samples for the Flames MRB18b and MRB26b at five downstream locations (h) from the nozzle.

h (mm)	MRB18b	MRB26b
15	5646	3514
22.5	4313	4434
30	4790	3927
60	2907	1682
90	1019	1040

kernels in each filter is the number of channels of the incoming layer. Then, the number of filters for each convolution is the number of channels of the outcoming layer. Hence, the total number of kernels for each convolution is the product of the number of channels at the incoming layer by the number of channels at the outcoming layer (e.g., at the first downsampling step following the input layer 8×64 kernels are used for the first convolution, while 64×64 kernels are used for the second convolution).

The upsampling path is a mirrored version of the downsampling path: it includes an upsampling operation which halves the number of feature channels, a concatenation operation which merges the corresponding feature map from the downsampling path, and two padded one-dimensional convolutions, each followed by a ReLU. At the final layer, a convolution with a kernel of 1 is used, with a Softmax activation to classify each 64-component feature vector to one of the eight combusion regimes. Tests have been performed with a single or three convolutions for each downsampling and upsampling step applied to the database, but as usual for the U-Net [27] architecture,

the best results are obtained with two convolutions.[1]

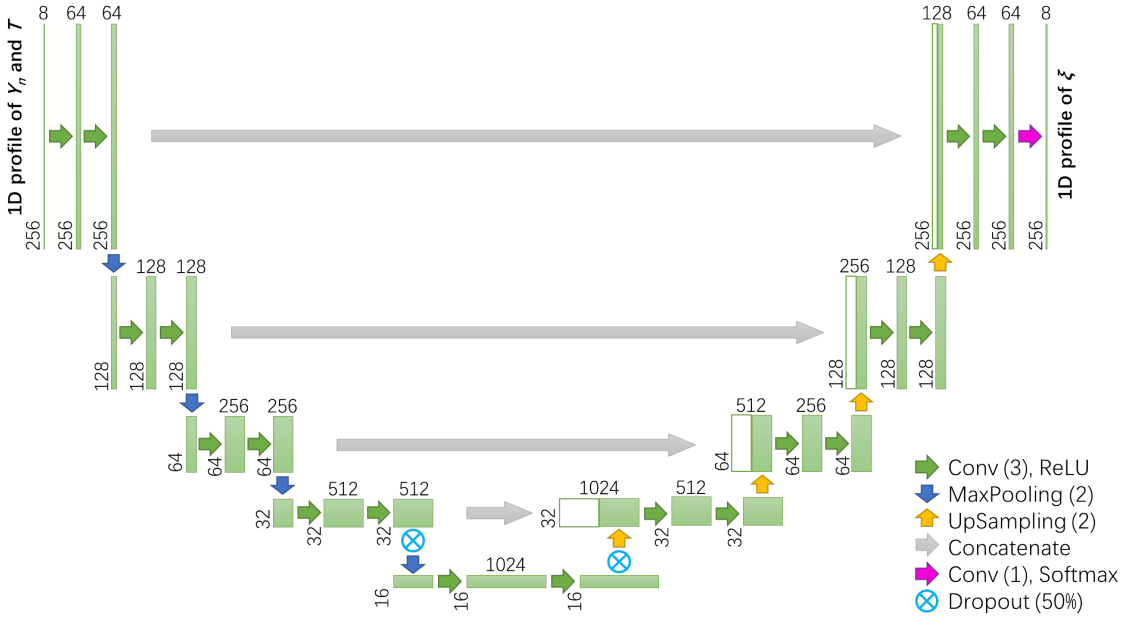

Figure 1: Structure of the CNN for combustion regime identification.

The resulting neural network contains 10,826,504 weights, which need to be trained. Three of the five locations (h = 15, 30 and 90 mm) of the MRB26b dataset are used for training the CNN. The remaining location of MRB26b (h = 22.5 and 60 mm) and all the 5 locations of MRB18b form the testing dataset to assess the performance of the CNN. (The corresponding codes are available as supplementary material.)

The training of the CNN is performed using the TensorFlow Python library with GPU support (`www.tensorflow.org`). A series of convolution, maxpooling and upsampling operations are performed iteratively, in which the neural weights are modified until a satisfying minimal departure is obtained between the "target" combustion regime index ξ and the CNNs predictions. The Adam optimizer [29] is applied with a sparse-categorical-crossentropy loss function comparing the prediction against the target.

To relieve overfitting, a drop-out rate of 50% is applied before the last maxpooling and the first upsampling operations (See Fig. 1). Data augmentation is also employed during training, to

[1] A more complex and advanced structure inspired by the fully convolutional DenseNet [28] has also been tested, without much improvement in prediction accuracy, but with a significantly higher computational cost.

increase the quality of the results. A mirror operation is first applied to each training sample line, to avoid the emergence of a preferential direction, then each original line now appears twice, in its original form and mirrored. Additionally, an uncorrelated random perturbation of 5% is added to each of these training sample lines, to build a new version of each original and mirrored lines with noise added. The "target" of the noise-added versions remains the same, thus mitigating the risk of overfitting. The final training dataset is the combination of the original, mirrored and noise-added versions, leading to a total of 33924 sample lines feeding the CNN for training.

The training is performed on a batch of 1024 lines, leading to 34 steps per "epoch"/iteration. The learning rate [20] is initially set to 0.0003 and decays versus the steps (n) according to

$$l_r = \frac{0.0003}{1.0 + 0.0001 \cdot n} \,. \tag{1}$$

The network is trained for 200 epochs to reach convergence, this requires about 45 minutes on an Nvidia GeForce GTX 1080 Ti GPU. The trained CNN reaches a prediction accuracy of 99.3% for the training database. Once trained, returning the combustion regime from an input line is almost instantaneous.

3. Results and discussion

3.1. CNN testing on the remaining location of MRB26b

After being trained on three of the five locations (h = 15, 30 and 90 mm) of the MRB26b dataset (Table 1), the CNN is tested at first on the remaining locations, h = 22.5 and 60 mm, of the same flame, which contains in total 6116 sample lines (Table 3), each with 256 pixels. By comparing, $\xi_{\mathrm{cnn}}(x)$, the combustion regime index predicted by the CNN to $\xi_{\mathrm{ref}}(x)$, the reference combustion regime index obtained from GFRI [11, 12], the CNN prediction is found to be 94.3% and 95.0% accurate[2] for h = 22.5 and 60 mm, respectively, which is satisfactory considering the complexity of the problem.

Figure 2 shows representative results for three sample lines from h = 22.5 mm and one from 60 mm of this MRB26b case. For the sample line 1 of h = 22.5 mm (Fig. 2(a)), a first premixed zone

[2]The dummy pixels are removed when calculating the accuracy.

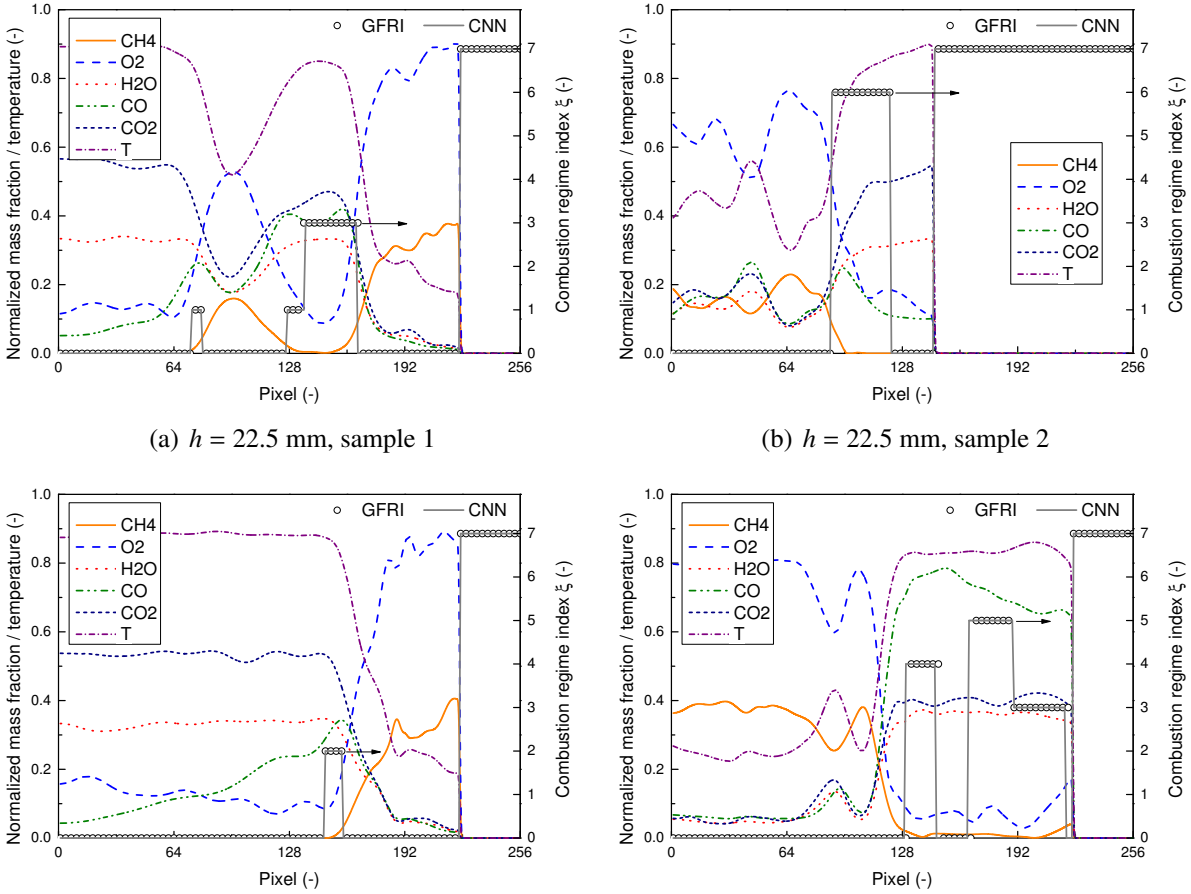

(a) h = 22.5 mm, sample 1

(b) h = 22.5 mm, sample 2

(c) h = 22.5 mm, sample 3

(d) h = 60 mm

Figure 2: Sample 1D lines at two h streamwise positions of MRB26b (Table 1). Left axis: Normalized mass fractions and temperature. Right axis: combustion regime index (Table 2). Circle: GFRI, one of every three pixels is plotted. Line: CNN.

(ξ = 1) around x = 75 pixels and a second one around x = 128 pixels followed by a multi-regime zone (ξ = 3) are well detected by the CNN. The profiles at the end of the sample line (x between 233 and 256 pixels) are dummy values to keep a uniform CNN input, which is indicated by ξ = 7 and is also well captured by the CNN. For the sample lines 2 (Fig. 2(b)) and 3 (Fig. 2(c)) of h = 22.5 mm, one lean back-supported zone (ξ = 6) and one dominatly premixed zone (ξ = 2) are well detected on each of the two sample lines, respectively. For the sample line of h = 60 mm (Fig. 2(d)), the prediction of CNN agrees well with the GFRI result, which detects a dominantly non-premixed zone (ξ = 4), a non-premixed zone (ξ = 5) and a multi-regime zone (ξ = 3) along the line.

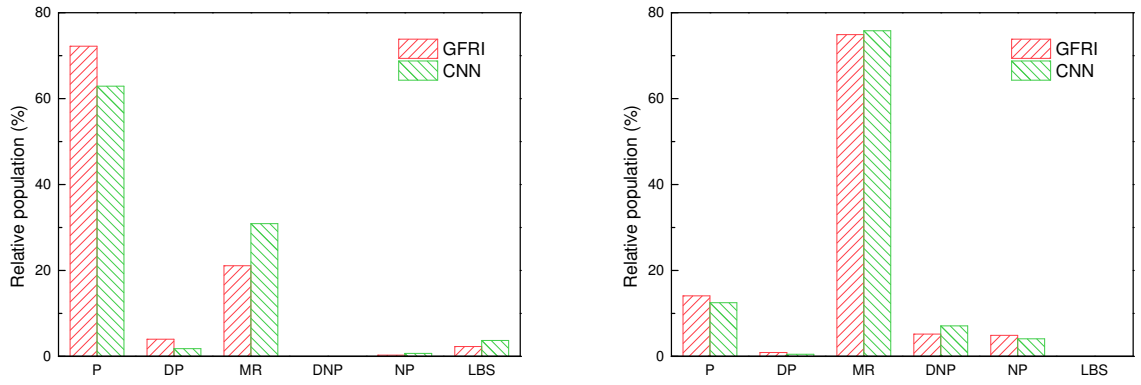

(a) h = 22.5 mm (b) h = 60 mm

Figure 3: Averaged distributions over sample lines of premixed (P), dominantly premixed (DP), multi-regime (MR), dominantly non-premixed (DNP), non-premixed (NP), and lean back-supported (LBS). (a) At the streamwise position h = 22.5 mm and (b) h = 60 mm of MRB26b. The predictions of CNN are compared to the reference results by the GFRI approach [11, 12]. Red: GFRI. Green: CNN.

Figure 3 compares the relative populations of combustion regimes over the locations h = 22.5 mm and 60 mm of MRB26b predicted by the CNN and the reference GFRI. The relative population of a combustion regime is computed as the number of pixels in this regime divided by the total number of pixels where combustion occurs, in other words the non burning (NB) and dummy pixels have been removed. At the location h = 22.5 mm (Fig. 3(a)), more than 60% of the reaction zones are identified with premixed characteristics, indicating that the flame is dominated by premixed combustion at this location which is not far from the nozzle. Further downstream, up to h = 60 mm (Fig. 3(b)), the multi-regime characteristics become the most significant with a relative population higher than 70%. This is in agreement with the MRB26b flame featuring a large region of mixtures above the rich flammability limit, thus promoting multi-regime combustion events. The lean back-supported regime is not found at this location (h = 60 mm), because it requires support from hot recirculating products, which is more likely to appear in the near-field region close to the nozzle, e.g., h = 22.5 mm (Fig. 3(a)). The predictions of the CNN on the distribution of various combustion regimes agree well with the reference GFRI calculations.

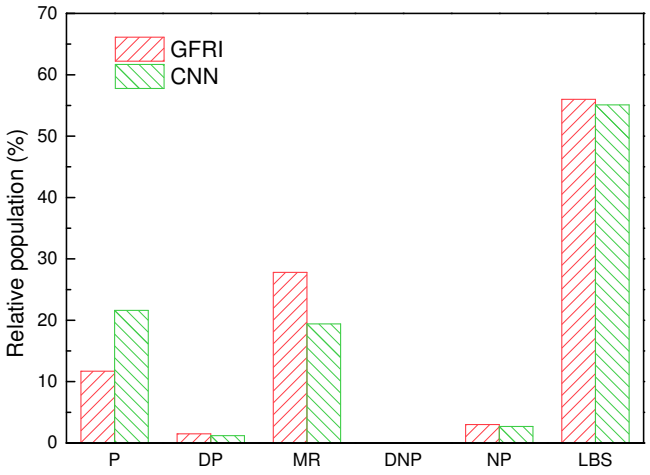

Figure 4: Averaged distributions over sample lines of premixed (P), dominantly premixed (DP), multi-regime (MR), dominantly non-premixed (DNP), non-premixed (NP), and lean back-supported (LBS) characteristics over all locations of MRB18b. The predictions of CNN are compared to the reference results by the GFRI approach [11, 12]. Red: GFRI. Green: CNN.

3.2. CNN testing on the unseen MRB18b dataset

The reliability of the CNN is now evaluated over all locations of the MRB18b dataset, which contains 18675 sample lines, each with 256 pixels. No location of this flame has been used for training. The predictions of the CNN on the relative populations of P, DP, MR, DNP, NP and LBS characteristics (Table 2) are summarized in Fig. 4. The flame structures of MRB18b are driven by lean back-supported, multi-regime, and premixed regimes. The CNN predictions achieve an overall good agreement against the GFRI results, with a good representation of the relative distribution of the combustion regimes over the six possibilities.

Figure 5 shows representative results for three sample lines from four different streamwise positions of the MRB18b case. The lean back-supported zone ($\xi = 6$) at $h = 15$ mm (Fig. 5(a)), two premixed zones ($\xi = 1$) at $h = 30$ mm (Fig. 5(b)), and one multi-regime zone ($\xi = 3$) and one non-premixed zone ($\xi = 5$) at $h = 90$ mm (Fig. 5(d)) are well captured by the CNN. At $h = 60$ mm (Fig. 5(c)), the CNN predicts a large entire dominatly premixed zone ($\xi = 2$) instead of two separate ones indicated by the GFRI, but this should be acceptable since the two separte ones are closely adjacent. These profiles have been chosen to illustrate the limitation of the approach observed for a few points. A mismatch is seen at $h = 15$ mm (Fig. 5(a)), where around $x =$

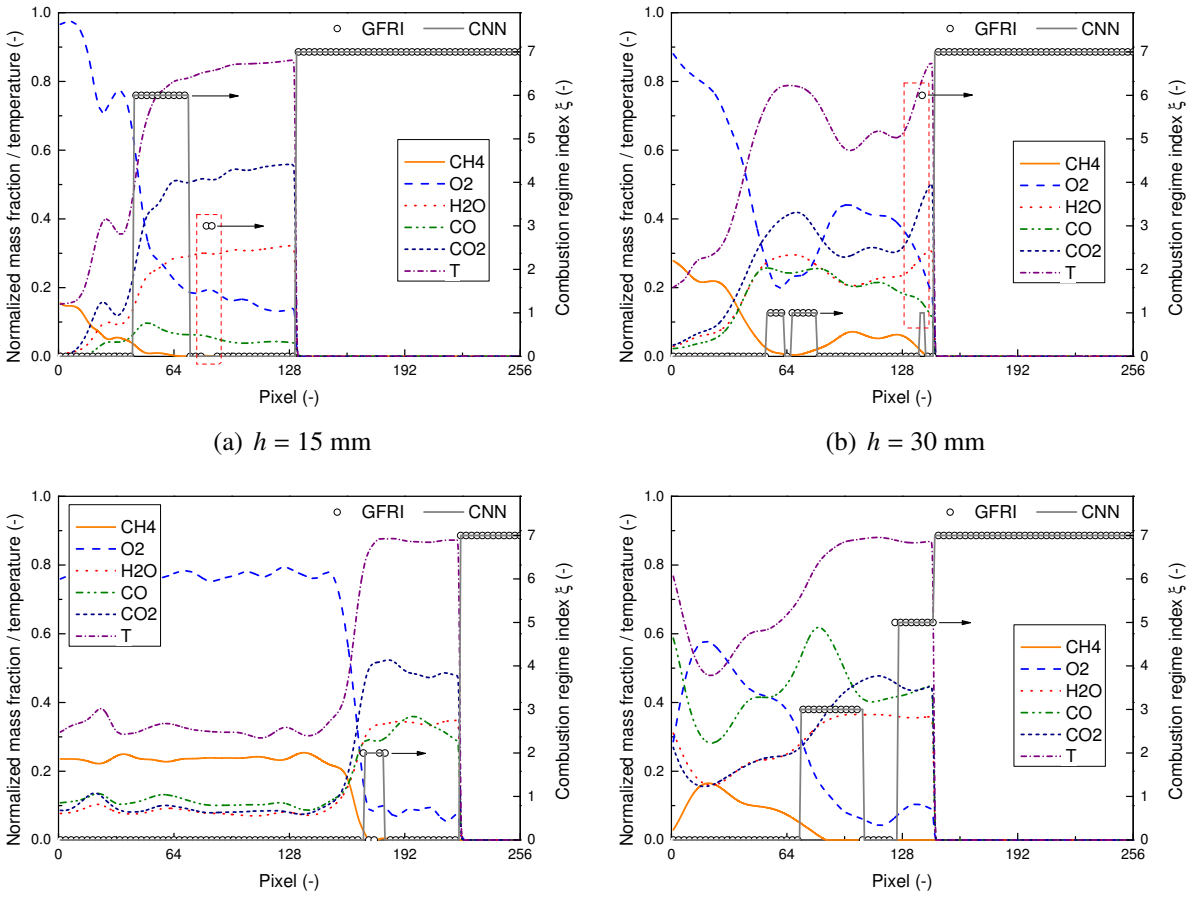

(a) h = 15 mm (b) h = 30 mm

(c) h = 60 mm (d) h = 90 mm

Figure 5: Sample 1D lines at four h streamwise positions of MRB18b (Table 1). Left axis: Normalized mass fractions and temperature. Right axis: combustion regime index (Table 2). Circle: GFRI, one of every three pixels is plotted. Line: CNN.

85 pixels of the line sample, the GFRI indicates a multi-regime zone, which is not detected by the CNN. Besides, at the x = 139 pixels of the line sample at h = 30 mm (Fig. 5(b)), the CNN predicts a premixed zone but the GFRI indicates a lean back-supported zone. Nevertheless, those mismatches contribute only a minor proportion to the overall combustion regime characteristics of an entire sample line.

By comparing the combustion regime index predicted by the CNN, $\xi_{\mathrm{cnn}}(x)$, to the reference combustion regime index, $\xi_{\mathrm{ref}}(x)$, determined by the GFRI approach [11, 12] at every pixel of the 18675 sample lines, 86.1% of prediction accuracy is found for this quite challenging complex multi-regime MRB18b dataset unseen during training. The CPU time required for CNN prediction

is of 2 s for the entire MRB18b dataset. Figure 6 displays the accuracy of the CNN over each of the five downstream locations of the MRB18b case. A precision of more than 85% is achieved for every location, which confirms the CNN accuracy.

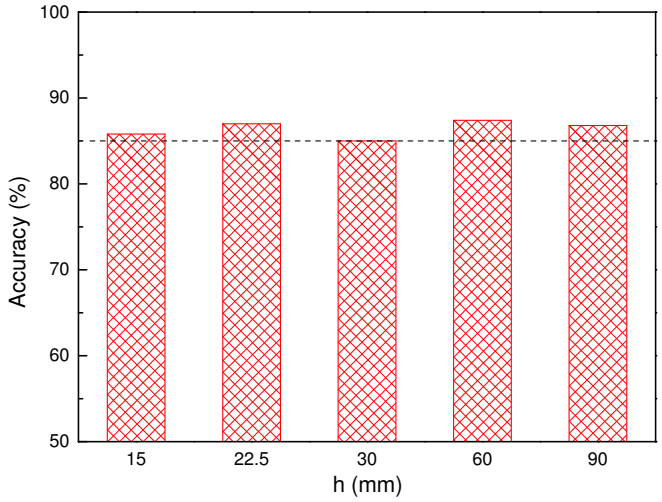

Figure 6: Prediction accuracy of the CNN over the five downstream locations of h = 15, 22.5, 30, 60 and 90 mm of the MRB18b dataset.The horizontal dashed line represents an accuracy of 85%.

4. Conclusions

A convolutional neural network (CNN) has been trained to determine combustion regimes in a methane-air turbulent flame from Raman/Rayleigh one-dimensional measurements of major species (H_2, O_2, CO, CO_2, CH_4, H_2O, and N_2) and temperature. The experimental data from a recently investigated multi-regime laboratory scale burner [12] are first processed with the gradient free regime identification (GFRI) method [11, 12], to generate a pixel-wise combustion regime database.

The CNN is trained at various heights along the burner axis for one operating condition and tested at two locations not included in the training. Then, the CNN is applied to a different burner operating condition, for which the free-stream equivalence ratios have been modified. Six classes of combustion regimes, including premixed (P), dominantly premixed (DP), multi-regime (MR), dominantly non-premixed (DNP), non-premixed (NP), and lean back-supported (LBS), are well

detected by the machine learning approach, with an accuracy of more than 85% for a dataset unseen during training. This accuracy needs to be put in perspective with the level of detail included in the analysis, which lead to consider six combustion sub-regimes, hence with a refinement that is not possible by most combustion regime identification procedures available so far. Indeed, usually three regimes (premixed, diffusion and partially premixed) only are distinguished by gradient or flux-based regime identification methods. Also, the combustion regime prediction in this study is pixel-wise, while most combustion regime identification methods usually operate over flow zones. In practice, the CNN can also be used to determine the dominant combustion regime observed in a single shot, or a series of shots defining a flow zone, still benefiting from the high level of confidence provided by GFRI initially used for training.

The training dataset of the present work is much smaller than typical deep learning datasets, even though returning quite accurate predictions. Compared to the most advanced combustion regime identification, as GFRI, the CNN is ultra-fast, making it possible to envision real-time combustion regime identification for advanced flame control, in order to mitigate pollutant emissions occurring under given local combustion regimes.

Once trained for a given range of fuel/air mixtures, it is expected that the neural network can be applied to different burner geometries. However, so far it cannot be expected very precise for free-stream equivalence ratios that would be far from those seen during the training phase.

Acknowledgments

Financial support is kindly acknowledged from the Deutsche Forschungsgemeinschaft (DFG, German Research Foundation) - Projektnummer 325144795. The first author is supported by ADEME (Agence de l'Environnement et de la Maîtrise de l'Energie, France) under the project IGAR (Injection de Gaz de Recycle) Grant Nb 1882C001. Computing resources were provided by CRIANN (`http://www.criann.fr`).

References

[1] H. Yamashita, M. Shimada, T. Takeno, A numerical study on flame stability at the transition point of jet diffusion flames, Symposium (International) on Combustion 26 (1) (1996) 27 – 34.

[2] Y. Mizobuchi, J. Shinjo, S. Ogawa, T. Takeno, A numerical on the formation of diffusion flame islands in a turbulent hydrogen jet lifted flame, Proc Combust Inst 30 (2005) 611–619.

[3] P. Domingo, L. Vervisch, J. Réveillon, DNS analysis of partially premixed combustion in spray and gaseous turbulent-flame bases stabilized in hot air, Combust. Flame 140 (3) (2005) 172–195.

[4] K. Luo, H. Pitsch, M. G. Pai, O. Desjardins, Direct numerical simulations and analysis of three-dimensional n-heptane spray flames in a model swirl combustor, Proc. Combust. Inst. 33 (2) (2011) 2143–2152.

[5] P. Domingo, L. Vervisch, K. Bray, Partially premixed flamelets in LES of nonpremixed turbulent combustion, Combustion Theory and Modelling 6 (4) (2002) 529–551.

[6] S. Nambully, P. Domingo, V. Moureau, L. Vervisch, A Filtered-Laminar-Flame PDF sub-grid scale closure for LES of premixed turbulent flames. Part II: Application to a stratified bluff-body burner, Combust. Flame 161 (7) (2014) 1775–1791.

[7] L. Ma, D. Roekaerts, Structure of spray in hot-diluted coflow flames under different coflow conditions: A numerical study, Combust. Flame 172 (2016) 20–37.

[8] P. Domingo, L. Vervisch, D. Veynante, Large-Eddy Simulation of a lifted methane-air jet flame in a vitiated coflow, Combust. Flame 152 (3) (2008) 415–432.

[9] E. Knudsen, H. Pitsch, A general flamelet transformation useful for distinguishing between premixed and non-premixed modes of combustion, Combust. Flame 156 (3) (2009) 678–696.

[10] D. A. Rosenberg, P. M. Allison, J. F. Driscoll, Flame index and its statistical properties measured to understand partially premixed turbulent combustion, Combust. Flame 162 (7) (2015) 2808–2882.

[11] S. Hartl, D. Geyer, A. Dreizler, G. Magnotti, R. S. Barlow, C. Hasse, Regime identification from Raman/Rayleigh line measurements in partially premixed flames, Combustion and Flame 189 (2018) 126 – 141.

[12] D. Butz, S. Hartl, S. Popp, S. Walther, R. S. Barlow, C. Hasse, A. Dreizler, D. Geyer, Local flame structure analysis in turbulent CH4/air flames with multi-regime characteristics, Combustion and Flame 210 (2019) 426 – 438.

[13] T. F. Lu, C. S. Yoo, J. H. Chen, C. K. Law, Three-dimensional direct numerical simulation of a turbulent lifted hydrogen jet flame in heated coflow: a chemical explosive mode analysis, Journal of Fluid Mechanics 652 (2010) 4564.

[14] S. Hartl, D. Geyer, C. Hasse, X. Zhao, H. Wang, R. S. Barlow, Assessing an experimental approach for chemical explosive mode and heat release rate using DNS data, Combustion and Flame 209 (2019) 214 – 224.

[15] S. Hartl, R. V. Winkle, D. Geyer, A. Dreizler, G. Magnotti, C. Hasse, R. Barlow, Assessing the relative importance of flame regimes in Raman/Rayleigh line measurements of turbulent lifted flames, Proceedings of the Combustion Institute 37 (2) (2019) 2297 – 2305.

[16] J. A. Blasco, N. Fueyo, C. Dopazo, J. Ballester, Modelling the temporal evolution of a reduced combustion chemical system with artificial neural network, Combust. Flame 113 (1-2) (1998) 38–52.

[17] L. L. Franke, A. K. Chatzopoulos, S. Rigopoulos, Tabulation of combustion chemistry via Artificial Neural Networks (ANNs): Methodology and application to LES-PDF simulation of Sydney flame L, Combust. Flame 185 (2017) 245–260.

[18] G. Aversano, A. Bellemans, Z. Li, A. Coussement, O. Gicquel, A. Parente, Application of reduced-order models based on PCA & Kriging for the development of digital twins of reacting flow applications, Computers & Chemical Engineering 121 (2) (2019) 422–441.

[19] Y. LeCun, Y. Bengio, G. Hinton, Deep learning, Nature 521 (2015) 436–444.

[20] H. H. Aghdam, E. J. Heravi, Guide to convolutional neural networks, Springer, New York, 2017.

[21] Z. M. Nikolaou, C. Chrysostomou, L. Vervisch, S. Cant, Progress Variable Variance and Filtered Rate Modelling Using Convolutional Neural Networks and Flamelet Methods, Flow Turbul. Combust. 103 (2) (2019) 485–501.

[22] C. J. Lapeyre, A. Misdariis, N. Cazard, D. Veynante, T. Poinsot, Training convolutional neural networks to estimate turbulent sub-grid scale reaction rates, Combust. Flame 203 (2019) 255–264.

[23] A. Seltz, P. Domingo, L. Vervisch, Z. M. Nikolaou, Direct mapping from LES resolved scales to filtered-flame generated manifolds using convolutional neural networks, Combust. Flame 210 (2019) 71–82.

[24] X. Zhu, Z. Cai, J. Wu, Y. Cheng, Q. Huang, Convolutional neural network based combustion mode classification for condition monitoring in the supersonic combustor, Acta Astronautica 159 (2019) 349–357.

[25] J. Long, E. Shelhamer, T. Darrell, Fully Convolutional Networks for Semantic Segmentation, in: The IEEE Conference on Computer Vision and Pattern Recognition (CVPR), 2015.

[26] V. Badrinarayanan, A. Kendall, R. Cipolla, SegNet: A Deep Convolutional Encoder-Decoder Architecture for Image Segmentation, IEEE Transactions on Pattern Analysis and Machine Intelligence 39 (12) (2017) 2481–2495.

[27] O. Ronneberger, P. Fischer, T. Brox, U-Net: Convolutional Networks for Biomedical Image Segmentation, in: N. Navab, J. Hornegger, W. M. Wells, A. F. Frangi (Eds.), Medical Image Computing and Computer-Assisted Intervention – MICCAI 2015, Springer International Publishing, Cham, 2015, pp. 234–241.

[28] S. Jegou, M. Drozdzal, D. Vazquez, A. Romero, Y. Bengio, The One Hundred Layers Tiramisu: Fully Convolutional DenseNets for Semantic Segmentation, in: The IEEE Conference on Computer Vision and Pattern Recognition (CVPR) Workshops, 2017.

[29] D. P. Kingma, J. Ba, Adam: A Method for Stochastic Optimization, arXiv e-prints (2014) arXiv:1412.6980.